Volume 23
Number 27
21 July 2025
Pages 6459-6654

Organic & Biomolecular Chemistry

rsc.li/obc

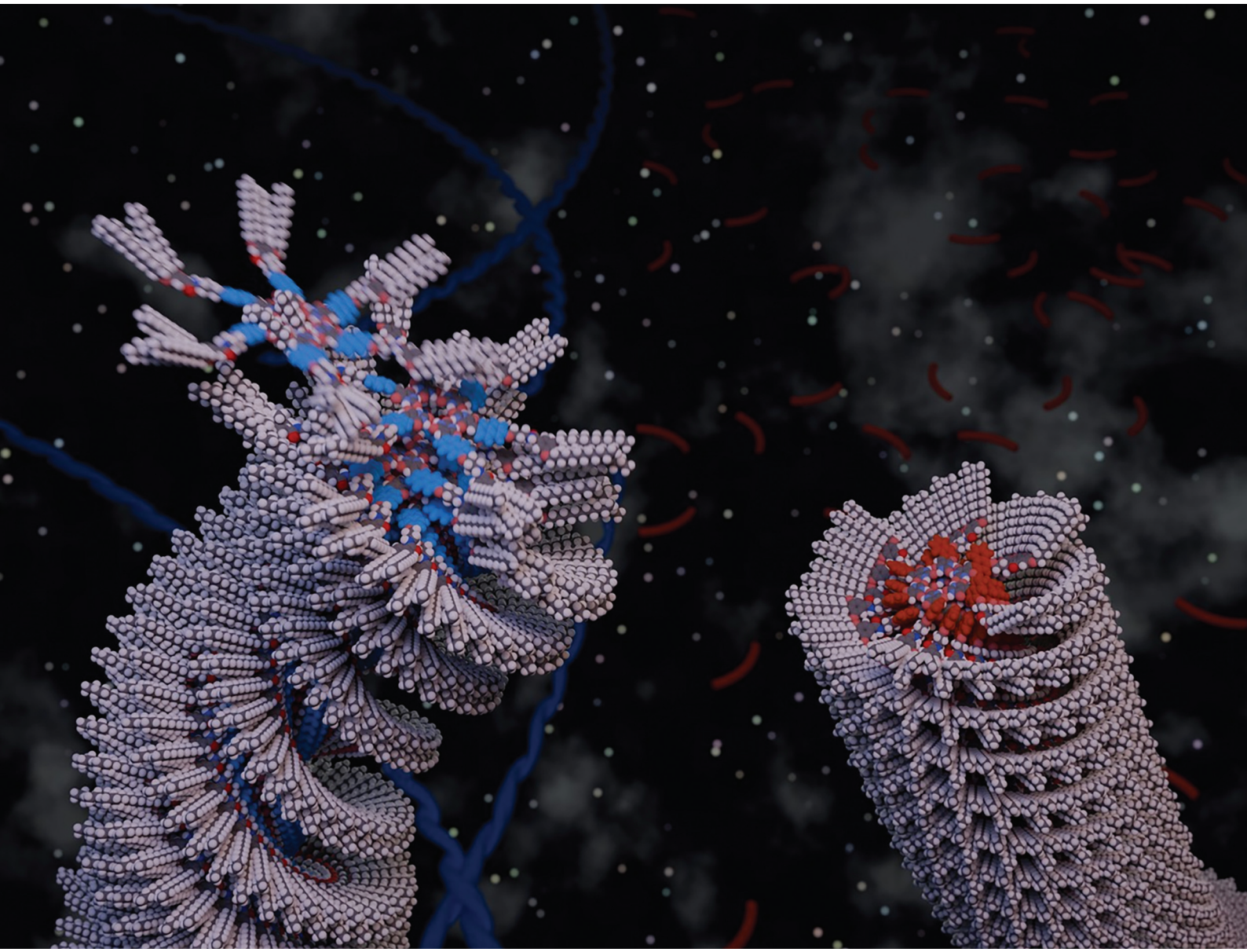

ISSN 1477-0520

ROYAL SOCIETY OF CHEMISTRY

COMMUNICATION
Shiki Yagai *et al.*
Competition and cooperation between steric hindrance and hydrogen bonding of supramolecular discs

Organic & Biomolecular Chemistry

ROYAL SOCIETY OF CHEMISTRY

COMMUNICATION

View Article Online
View Journal | View Issue

Cite this: *Org. Biomol. Chem.*, 2025, **23**, 6516

Received 12th April 2025,
Accepted 8th May 2025

DOI: 10.1039/d5ob00609k

rsc.li/obc

Competition and cooperation between steric hindrance and hydrogen bonding of supramolecular discs†

Yuhei Yamada, ‡[a] Shunsuke Kakinuma,‡[a] Hiroki Hanayama,[b] Sougata Datta [c] and Shiki Yagai *[b,c]

We previously reported supramolecular polymers formed by π–π stacking between disc-shaped hexamers (rosettes) of barbituric acid-functionalized π-conjugated molecules. Herein, we investigated the impact of amide-mediated hydrogen bonding along two types of polymer backbones formed by distinct stacking of rosettes. The stabilization of the hydrogen bonds strongly depends on the intrinsic stacking arrangement of rosettes, which competes with the amide hydrogen-bonding.

Supramolecular polymers are stimuli-responsive polymeric materials obtained by linking small molecules through robust non-covalent interactions.[1,2] Initially, supramolecular polymer research was predominantly focused on flexible supramolecular polymers comprising multiple hydrogen bonding sites[3–6] or host–guest pairs[7–10] connected by flexible side chains. However, recent efforts have increasingly explored designs involving the stacking of disc-shaped aromatic molecules *via* multiple peripheral hydrogen bonds.[11–14] A distinctive feature of these systems is the cooperative nature of the supramolecular polymerisation process: an initial aggregation of a critical number of monomers (nucleation phase) locks their molecular conformations, thereby facilitating the subsequent addition of further monomers (elongation phase).[15–17] This cooperative assembly has advanced our understanding of metastable states, pathway complexity,[18–20] precision supramolecular polymerisation,[21–23] supramolecular polymorphism,[24,25] and hierarchical assembly,[26–28] thereby promoting broader research related to molecular self-assembly into solid-state materials.

For disc-shaped molecules predominantly employing extended π-conjugated systems, π-stacking further enhances cooperativity.[29] Such extended π-conjugated systems can be synthesized directly or achieved through pseudo-extension mediated by multiple hydrogen bonds.[30–34] Notably, in the latter scenario, hydrogen bonding occurs orthogonally rather than along the polymer growth axis. Our research has long focused on π-conjugated molecules functionalized with a barbituric acid group and an alkyl tail. These molecules form cyclic hexameric assemblies (rosettes, Fig. 1a) *via* hydrogen bonding between barbituric acid moieties, subsequently stacking to yield supramolecular polymers.[31,35] A particularly intriguing aspect is the profound influence that rosette geometry and the dipole moments of barbituric acid-functionalized π-conjugated units exert on the stacking modes of these rosettes.[25,36,37]

Clear examples are provided by compounds **1** and **2**, based on 1,4- and 2,6-disubstituted naphthalene, respectively (Fig. 1b).[36] Rosettes derived from compound **1** feature protruding naphthalene units, necessitating rotational offsets during stacking to mitigate steric hindrance. Consequently, naphthalene units stack in a helical, face-to-face (H-type) arrangement, resulting in cylindrical supramolecular polymers that extend up to micrometre lengths even at sub-millimolar concentrations (Fig. 1c). In contrast, rosettes of compound **2**, devoid of significant steric hindrance from naphthalene units, consistently stack with combined rotational and translational offsets determined by their dipole moments. This stacking arrangement inherently induces curvature in the main polymer chain, generating uniform ring structures (Fig. 1c). Thus, the extent of interlocking and steric constraints inherent to these non-planar rosettes fundamentally drives their stacking patterns.

In this study, we aimed to strategically enhance the stacking interactions of rosettes formed by **1** and **2** by introducing additional hydrogen bonds along the polymer backbone

[a]*Division of Advanced Science and Engineering, Graduate School of Engineering, Chiba University, 1-33 Yayoi-cho, Inage-ku, Chiba 263-8522, Japan*
[b]*Department of Applied Chemistry and Biotechnology, Graduate School of Engineering, Chiba University, 1-33 Yayoi-cho, Inage-ku, Chiba 263-8522, Japan*
[c]*Institute for Advanced Academic Research (IAAR), Chiba University, 1-33 Yayoi-cho, Inage-ku, Chiba 263-8522, Japan. E-mail: yagai@faculty.chiba-u.jp*

†Electronic supplementary information (ESI) available: General information, synthesis, structural characterization data, photophysical and morphological studies. See DOI: https://doi.org/10.1039/d5ob00609k

‡These authors contributed equally to this work.

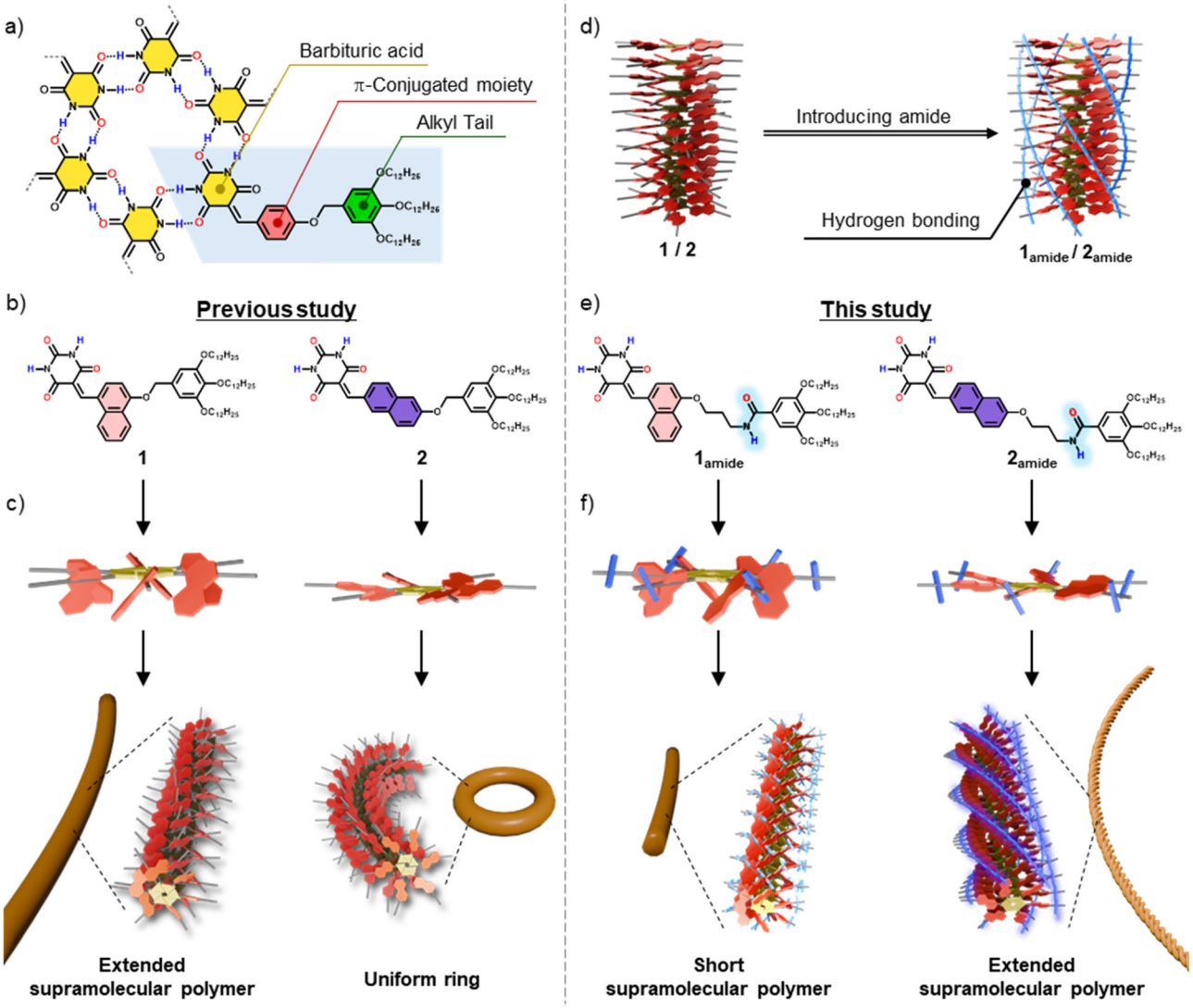

Fig. 1 (a) Hydrogen-bonded rosette composed of barbituric acid moieties. (b) Molecular structures of **1** and **2**. (c) Schematic representations of geometrical features of rosettes composed of **1** and **2** and supramolecular polymerisations these rosettes. (d) Schematic representations of hydrogen-bonded network of amide groups along the rosette stacking. (e) Molecular structures of $\mathbf{1}_{amide}$ and $\mathbf{2}_{amide}$. (f) Schematic representations of geometrical features of rosettes composed of $\mathbf{1}_{amide}$ and $\mathbf{2}_{amide}$ and supramolecular polymerisations of these rosettes.

(Fig. 1d). To achieve this, we synthesized compounds $\mathbf{1}_{amide}$ and $\mathbf{2}_{amide}$, incorporating an amide group through a $-(CH_2)_3-$ spacer (Fig. 1e). The introduction of the spacer was based on a previous report suggesting that when the hydrogen-bonding site is too close to the aromatic moiety, it tends to form hydrogen bonds with the barbituric acid unit, thereby promoting dimerization and the formation of sheet-like structures instead of rosette assemblies.[38] Interestingly, the introduction of an amide group to the 1,4-naphthalene derivative ($\mathbf{1}_{amide}$), which originally formed elongated supramolecular polymers through rotational offsets, resulted in the formation of relatively shorter supramolecular polymers (Fig. 1f). Conversely, for the 2,6-naphthalene derivative ($\mathbf{2}_{amide}$), which originally formed ring structures due to translational offsets, the introduced amide functionality facilitated elongation into extended supramolecular polymers (Fig. 1f). These contrasting results clearly suggest that the introduction of amide hydrogen bonding sites does not universally promote supramolecular polymer elongation; rather, compatibility between supramolecular monomers and the introduced interactive sites plays a critical role.

The assembly processes of $\mathbf{1}_{amide}$ and $\mathbf{2}_{amide}$ were investigated by dissolving each compound in methylcyclohexane (MCH) at 50 μM, heating to 100 °C, and then cooling to 20 °C at 1 °C min^{-1}. Upon cooling, the broad major absorption band of $\mathbf{1}_{amide}$ (λ_{max} = 425 and 438 nm) shifted to a sharp band (λ_{max} = 421 nm). This change was accompanied by the appearance of a new weak absorption at 500 nm (Fig. 2a). Conversely,

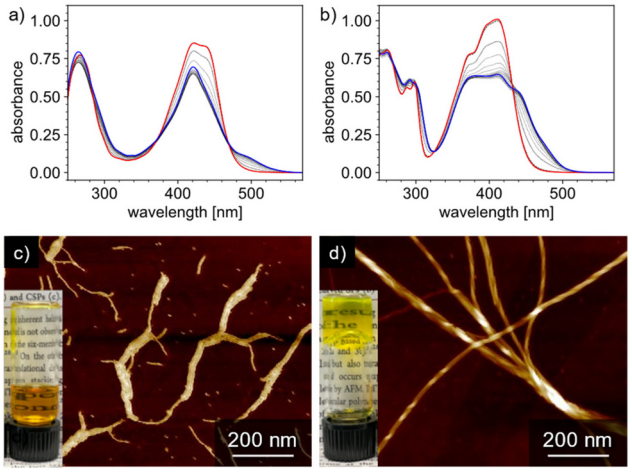

Fig. 2 (a and b) Temperature-dependent changes in the UV-Vis spectra of (a) $\mathbf{1}_{amide}$ and (b) $\mathbf{2}_{amide}$ (c = 50 μM) in MCH during cooling from 100 °C (red) to 20 °C (blue) at a rate of 1 °C min^{-1} at 5 °C intervals. (c and d) AFM images of nanofibers formed by (c) $\mathbf{1}_{amide}$ and (d) $\mathbf{2}_{amide}$. Insets show photographs of a solution of $\mathbf{1}_{amide}$ and a gel of $\mathbf{2}_{amide}$ in MCH (c = 1 mM).

$\mathbf{2}_{amide}$ exhibited a new absorption band emerging between 450 and 500 nm (Fig. 2b). These spectral changes closely resemble those observed in **1** and **2** without amide groups, suggesting face-to-face (H-type) and offset (J-type) stacking of naphthalene moieties, respectively.[36]

To comparatively evaluate the contribution of amide–amide hydrogen bonding during supramolecular polymerisation of $\mathbf{1}_{amide}$ and $\mathbf{2}_{amide}$, thermodynamic parameters were assessed using temperature-dependent absorption measurements. Solutions of each compound in MCH were prepared at various concentrations and cooled at a rate of 1 °C min^{-1} (Fig. S1†). Plotting absorption changes *versus* temperature revealed non-sigmoidal temperature dependence, indicative of a cooperative assembly mechanism involving distinct nucleation and elongation processes (Fig. S2 and S3†). In the case of $\mathbf{2}_{amide}$, a weak secondary transition was observed at lower temperatures, indicative of a secondary assembly process (Fig. S3†). Since heating curves displayed similar temperature dependence (Fig. S1†), the cooling processes could be considered thermodynamically controlled. Therefore, the cooling curves were global-fitted using a cooperative supramolecular polymerisation model[16] and melting curve analysis,[39] and standard enthalpy and entropy changes were estimated directly as shared parameters (Table 1 and Fig. S2, S3†). Standard

Table 1 Thermodynamic parameters of supramolecular polymerisation of $\mathbf{1}_{amide}$, $\mathbf{2}_{amide}$, **1** [40] and **2** [41]

	$\Delta H°$ (kJ mol^{-1})	$\Delta S°$ (mol^{-1} K^{-1})
$\mathbf{1}_{amide}$	−96	−180
$\mathbf{2}_{amide}$	−117	−238
1	−81	−173
2	−72	−139

enthalpy changes ($\Delta H°$) were determined to be −96 kJ mol^{-1} for $\mathbf{1}_{amide}$ and −117 kJ mol^{-1} for $\mathbf{2}_{amide}$, indicating that the latter with 2,6-disubstituted naphthalene forms stronger intermolecular interactions. Correspondingly, $\mathbf{2}_{amide}$ exhibited a greater standard entropy loss ($\Delta S°$ = −238 J mol^{-1} K^{-1}) compared to $\mathbf{1}_{amide}$ ($\Delta S°$ = −180 J mol^{-1} K^{-1}), signifying more ordered conformations to form optimum intermolecular interactions. Remarkably, these thermodynamic parameters contrast with the results observed for parent naphthalene derivatives **1** and **2**, highlighting that the introduction of amide groups inhibits stacking for the 1,4-naphthalene rosette but substantially promotes stacking for the 2,6-naphthalene rosette.

Consistent with these results, atomic force microscopy (AFM) observations revealed notable differences in the aggregate morphologies of $\mathbf{1}_{amide}$ and $\mathbf{2}_{amide}$. When a cooled solution of $\mathbf{1}_{amide}$ was spin-coated onto highly oriented pyrolytic graphite (HOPG) substrate, AFM revealed bundled fibres approximately 6.6 nm in diameter and 100–600 nm in length, which are relatively short compared to supramolecular polymers of parent compound **1** under comparable conditions (Fig. 2c and S4a†). In stark contrast, $\mathbf{2}_{amide}$ at 70 °C exhibited single linear fibres (Fig. S5a and b†), which showed progressive twisting and bundling upon cooling to 50 °C (Fig. S5c and d†). The higher-order transitions are likely associated with the secondary transition observed in the lower temperature regime. At 20 °C, helically twisted fibres exceeding 4 μm in length were predominantly observed, with the thinnest fibres measuring approximately 5 nm in width (Fig. 2d and S4b†). Reflecting these mesoscopic structural differences, high-concentration (1 mM) MCH solutions remained fluid for $\mathbf{1}_{amide}$, whereas gelation was observed for $\mathbf{2}_{amide}$ (insets in Fig. 2c and d). Comparing these supramolecular polymer structures with those of parent compounds **1** and **2**, which form elongated fibres and closed rings, respectively,[36] reveals that the observed differences clearly correlate with thermodynamic parameters. Thus, the mismatch of hydrogen bonding due to rotational offset likely weakened supramolecular polymerisation of the rosette of $\mathbf{1}_{amide}$, whereas the absence of geometric constraints allowed robust, well-aligned hydrogen bonding of the rosette of $\mathbf{2}_{amide}$, promoting substantial elongation.

To verify the hypothesis regarding hydrogen-bond matching and rosette core alignment, FT-IR spectroscopy was employed to compare the strength of hydrogen bonds between amide groups within the supramolecular polymers. FT-IR spectra of monomeric solutions of $\mathbf{1}_{amide}$ and $\mathbf{2}_{amide}$ in $CHCl_3$ exhibited characteristic amide N–H stretching vibrations around 3450 cm^{-1} and carbonyl C=O stretching vibrations at 1675 cm^{-1}, which were supported by DFT calculations corrected by a linear correlation (Fig. S6†).[42] In contrast, FT-IR spectra in MCH solutions showed a shift of these stretching vibrations to lower wavenumbers. Notably, the shift of N–H stretching vibrations observed for $\mathbf{1}_{amide}$ was smaller and the band was broader than for $\mathbf{2}_{amide}$, indicating less uniform and weaker hydrogen bonding in $\mathbf{1}_{amide}$. These results strongly support the hypothesis that differences in rosette core align-

ment critically influence the efficiency and uniformity of hydrogen bonding interactions within these supramolecular polymers.

Conclusions

In conclusion, although numerous disc-based supramolecular polymers have been developed using amide functionalization of disc-shaped aromatic molecules, our results clearly demonstrate that introducing amide groups into these building blocks does not necessarily promote supramolecular polymerisation. The formation of thermodynamically stable hydrogen bonds critically depends on the alignment of the amide groups of disc-shaped (supra)molecules, which may conflict with their inherently stable stacking arrangement. When these two intermolecular interactions compete, amide introduction may even deteriorate the intrinsic stacking ability of disc-shaped molecules. Our findings highlight a design strategy for stabilizing barbiturate-directed supramolecular polymers *via* orthogonal hydrogen bonding, which may facilitate the development of novel mesoscopic materials with curved supramolecular chains characteristic of barbituric acid derivatives.[27]

Data availability

The data that support the findings of this study are available in the ESI.†

Conflicts of interest

There are no conflicts to declare.

Acknowledgements

This work was supported by the Japan Society for the Promotion for Science (JSPS) KAKENHI grant no. JP23H04873 in a Grant-in-Aid for Transformative Research Areas "Materials Science of Meso-Hierarchy".

References

1 L. Brunsveld, B. J. B. Folmer, E. W. Meijer and R. P. Sijbesma, *Chem. Rev.*, 2001, **101**, 4071–4098.
2 T. Aida, E. W. Meijer and S. I. Stupp, *Science*, 2012, **335**, 813–817.
3 R. P. Sijbesma, F. H. Beijer, L. Brunsveld, B. J. B. Folmer, J. H. K. K. Hirschberg, R. F. M. Lange, J. K. L. Lowe and E. W. Meijer, *Science*, 1997, **278**, 1601–1604.
4 R. F. M. Lange, M. van Gurp and E. W. Meijer, *J. Polym. Sci., Part A: Polym. Chem.*, 1999, **37**, 3657–3670.
5 V. Berl, M. Schmutz, M. J. Krische, R. G. Khoury and J.-M. Lehn, *Chem. – Eur. J.*, 2002, **8**, 1227–1244.
6 S. Yagai, *J. Photochem. Photobiol., C*, 2006, **7**, 164–182.
7 T. Haino, *Polym. J.*, 2013, **45**, 363–383.
8 D. Xia, P. Wang, X. Ji, N. M. Khashab, J. L. Sessler and F. Huang, *Chem. Rev.*, 2020, **120**, 6070–6123.
9 G. Gattuso, A. Notti, A. Pappalardo, M. F. Parisi, I. Pisagatti, S. Pappalardo, D. Garozzo, A. Messina, Y. Cohen and S. Slovak, *J. Org. Chem.*, 2008, **73**, 7280–7289.
10 R. K. Castellano, R. Clark, S. L. Craig, C. Nuckolls and J. Rebek, *Proc. Natl. Acad. Sci. U. S. A.*, 2000, **97**, 12418–12421.
11 S. Díaz-Cabrera, Y. Dorca, J. Calbo, J. Aragó, R. Gómez, E. Ortí and L. Sánchez, *Chem. – Eur. J.*, 2018, **24**, 2826–2831.
12 M. M. J. Smulders, A. P. H. J. Schenning and E. W. Meijer, *J. Am. Chem. Soc.*, 2008, **130**, 606–611.
13 S. Cantekin, T. F. A. De Greef and A. R. A. Palmans, *Chem. Soc. Rev.*, 2012, **41**, 6125–6137.
14 S. H. Jung, D. Bochicchio, G. M. Pavan, M. Takeuchi and K. Sugiyasu, *J. Am. Chem. Soc.*, 2018, **140**, 10570–10577.
15 F. Oosawa and M. Kasai, *J. Mol. Biol.*, 1962, **4**, 10–21.
16 D. Zhao and J. S. Moore, *Org. Biomol. Chem.*, 2003, **1**, 3471–3491.
17 M. M. J. Smulders, M. M. L. Nieuwenhuizen, T. F. A. de Greef, P. van der Schoot, A. P. H. J. Schenning and E. W. Meijer, *Chem. – Eur. J.*, 2010, **16**, 362–367.
18 I. V. Baskakov, G. Legname, M. A. Baldwin, S. B. Prusiner and F. E. Cohen, *J. Biol. Chem.*, 2002, **277**, 21140–21148.
19 P. A. Korevaar, S. J. George, A. J. Markvoort, M. M. J. Smulders, P. A. J. Hilbers, A. P. H. J. Schenning, T. F. A. de Greef and E. W. Meijer, *Nature*, 2012, **481**, 492–496.
20 J. Matern, Y. Dorca, L. Sánchez and G. Fernández, *Angew. Chem., Int. Ed.*, 2019, **58**, 16730–16740.
21 M. Wehner and F. Würthner, *Nat. Rev. Chem.*, 2019, **4**, 38–53.
22 S. Ogi, K. Sugiyasu, S. Manna, S. Samitsu and M. Takeuchi, *Nat. Chem.*, 2014, **6**, 188–195.
23 J. Kang, D. Miyajima, T. Mori, Y. Inoue, Y. Itoh and T. Aida, *Science*, 2015, **347**, 646–651.
24 M. Wehner, M. I. S. Röhr, M. Bühler, V. Stepanenko, W. Wagner and F. Würthner, *J. Am. Chem. Soc.*, 2019, **141**, 6092–6107.
25 C. Otsuka, S. Takahashi, A. Isobe, T. Saito, T. Aizawa, R. Tsuchida, S. Yamashita, K. Harano, H. Hanayama, N. Shimizu, H. Takagi, R. Haruki, L. Liu, M. J. Hollamby, T. Ohkubo and S. Yagai, *J. Am. Chem. Soc.*, 2023, **145**, 22563–22576.
26 S. Datta, M. L. Saha and P. J. Stang, *Acc. Chem. Res.*, 2018, **51**, 2047–2063.
27 S. Datta, H. Itabashi, T. Saito and S. Yagai, *Nat. Chem.*, 2025, **17**, 477–492.
28 V. Vázquez-González, M. J. Mayoral, R. Chamorro, M. M. R. M. Hendrix, I. K. Voets and D. González-Rodríguez, *J. Am. Chem. Soc.*, 2019, **141**, 16432–16438.
29 T. F. A. de Greef, M. M. J. Smulders, M. Wolffs, A. P. H. J. Schenning, R. P. Sijbesma and E. W. Meijer, *Chem. Rev.*, 2009, **109**, 5687–5754.

30 V. Vázquez-González, M. J. Mayoral, F. Aparicio, P. Martínez-Arjona and D. González-Rodríguez, *ChemPlusChem*, 2021, **86**, 1087–1096.
31 S. Datta, S. Takahashi and S. Yagai, *Acc. Mater. Res.*, 2022, **3**, 259–271.
32 S. Yagai, *Bull. Chem. Soc. Jpn.*, 2015, **88**, 28–58.
33 H. Fenniri, P. Mathivanan, K. L. Vidale, D. M. Sherman, K. Hallenga, K. V. Wood and J. G. Stowell, *J. Am. Chem. Soc.*, 2001, **123**, 3854–3855.
34 M. González-Sánchez, M. J. Mayoral, V. Vázquez-González, M. Paloncýová, I. Sancho-Casado, F. Aparicio, A. de Juan, G. Longhi, P. Norman, M. Linares and D. González-Rodríguez, *J. Am. Chem. Soc.*, 2023, **145**, 17805–17818.
35 S. Yagai, Y. Kitamoto, S. Datta and B. Adhikari, *Acc. Chem. Res.*, 2019, **52**, 1325–1335.
36 S. Yagai, Y. Goto, X. Lin, T. Karatsu, A. Kitamura, D. Kuzuhara, H. Yamada, Y. Kikkawa, A. Saeki and S. Seki, *Angew. Chem., Int. Ed.*, 2012, **51**, 6643–6647.
37 C. Otsuka, S. Imai, T. Ohkubo and S. Yagai, *Chem. Commun.*, 2024, **60**, 1108–1111.
38 T. Aizawa, K. Aratsu, S. Datta, T. Mashimo, T. Seki, T. Kajitani, F. Silly and S. Yagai, *Chem. Commun.*, 2020, **56**, 4280–4283.
39 H. M. M. ten Eikelder, A. J. Markvoort, T. F. A. de Greef and P. A. J. Hilbers, *J. Phys. Chem. B*, 2012, **116**, 5291–5301.
40 M. Yamauchi, B. Adhikari, D. D. Prabhu, X. Lin, T. Karatsu, T. Ohba, N. Shimizu, H. Takagi, R. Haruki, S. Adachi, T. Kajitani, T. Fukushima and S. Yagai, *Chem. – Eur. J.*, 2017, **23**, 5270–5280.
41 K. Aratsu, R. Takeya, B. R. Pauw, M. J. Hollamby, Y. Kitamoto, N. Shimizu, H. Takagi, R. Haruki, S. Adachi and S. Yagai, *Nat. Commun.*, 2020, **11**, 1623.
42 M. Katari, E. Nicol, V. Steinmetz, G. van der Rest, D. Carmichael and G. Frison, *Chem. – Eur. J.*, 2017, **23**, 8414–8423.